Available online at www.sciencedirect.com
SCIENCE DIRECT®
Chemical Physics Letters 393 (2004) 361–366
CHEMICAL PHYSICS LETTERS
www.elsevier.com/locate/cplett

The C 1s NEXAFS spectrum of benzene below threshold: Rydberg or valence character of the unoccupied σ-type orbitals

R. Püttner [a,*], C. Kolczewski [b], M. Martins [a,1], A.S. Schlachter [c], G. Snell [c,d], M. Sant'Anna [c,2], J. Viefhaus [b], K. Hermann [b], G. Kaindl [a]

[a] Institut für Experimentalphysik, Fachbereich Physik, Freie Universität Berlin, Arnimallee 14, D-14195 Berlin-Dahlem, Germany
[b] Fritz-Haber-Institut der Max-Planck-Gesellschaft, Faradayweg 4-6, 14195 Berlin, Germany
[c] Advanced Light Source, Lawrence Berkeley National Laboratory, Berkeley, CA 94720, USA
[d] Department of Physics, Western Michigan University, Kalamazoo, MI 49008-5151, USA

Received 28 April 2004; in final form 9 June 2004

Abstract

High-resolution C 1s near edge X-ray absorption fine structure (NEXAFS) spectra of benzene and benzene-d_6 were measured and compared with the results of state-of-the-art density functional theory (DFT) calculations demonstrating excellent agreement. The spectrum below threshold is dominated by four resonances, each two of them with σ- and π-type final-state orbitals. The π-type resonances have been ascribed in previous work unanimously to antibonding valence orbitals while the character of the σ-type resonances is still the subject of discussion. Based on the present theoretical results and the observed vibrational fine structures both σ-type orbitals are assigned to be valence type with minor admixtures of Rydberg character.

1. Introduction

Near edge X-ray absorption fine structure (NEXAFS) spectroscopy is a well-established and powerful tool for probing unoccupied orbitals and bands in molecules [1], adsorbates on substrates [2–4], and solids [5]. The method is element specific and sensitive to the chemical environment of an atom, and is therefore well-suited to provide useful information on the local bonding situation. For adsorbate systems additional details about the adsorption geometry can be obtained. Technological improvements such as third-generation synchrotron radiation facilities and advanced monochromators have been utilized to obtain high-resolution NEXAFS spectra, partly even with resolved vibrational fine structure [6–8].

Benzene is a molecule of considerable economic interest and also plays an important role in a number of every day-life situations, e.g. in improving the octane rating of fuel. It is also used as a solvent and for the synthesis of a number of aromatic molecules, e.g. aniline, styrene, certain synthetics, azo-dyes, and detergents.

The highly symmetric molecule benzene is of particular interest in the context of NEXAFS spectroscopy since it serves as a prototype for a large number of aromatic molecules and building blocks in polymers. Therefore, its experimental spectrum has been studied widely in the gas-phase [9,10], in the condensed-phase [11], and as adsorbed molecules [3]. Considering the importance of benzene, it is astonishing that two of the resonances observed in the C 1s NEXAFS spectrum below the ionization threshold (peaks B and C in Fig. 1) are still subject to debate. Some authors assign these resonances to C $1s^{-1}3s$ and C $1s^{-1}3p$ Rydberg excitations [10], while others argue with partial valence char-

* Corresponding author. Fax: +49-30-838-56560.
E-mail address: puettner@physik.fu-berlin.de (R. Püttner).
[1] Present address: Institut für Experimentalphysik, Universität Hamburg, Luruper Chaussee 149, D-22761 Hamburg, Germany.
[2] Present address: Instituto de Fysica, Universidade Federal do Rio de Janeiro, Caixa Postal 68528, Rio de Janeiro, RJ 21941-972, Brazil.

0009-2614/$ - see front matter © 2004 Elsevier B.V. All rights reserved.
doi:10.1016/j.cplett.2004.06.053

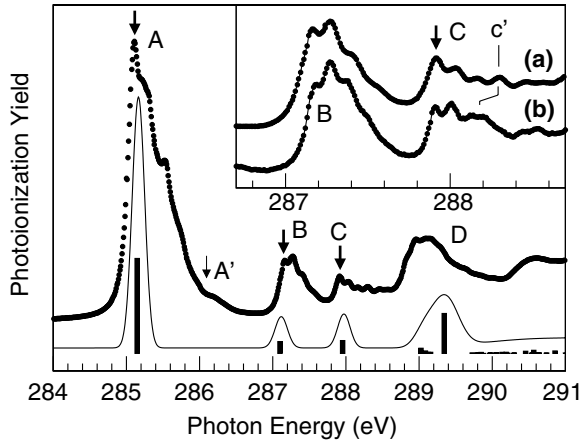

Fig. 1. Photoionization spectrum of benzene below the C 1s ionization threshold. The theoretical spectrum (solid line) is shifted by 0.2 eV to higher energies for better visual comparison with the experimental results (data points). The vertical bars indicate the calculated energy positions and intensities of the resonances. The thick vertical arrows indicate the energy positions for the $v'' = 0 \rightarrow v' = 0$ transitions given in Table 1 and the thin vertical arrow at 286.05 eV indicates the calculated energy position of the dipole-forbidden C $1s^{-1}\pi^*a_2$ transition A′ (see text). The inset shows the vibrational fine structure of peaks B and C in (a) benzene and (b) benzene-d_6 in detail. For better comparison the spectrum of benzene-d_6 was shifted by 50 meV to higher energies.

acter of these orbitals [11,12]. Knowledge of the true character of the two resonances is particularly interesting for a correct interpretation of the results of adsorption studies that investigate the influence of different substrates on the electronic properties of the adsorbate. Such studies have been performed for benzene on a large number of different substrates. For example, Weiss et al. [3] studied the NEXAFS spectrum of a monolayer of benzene on different close-packed metal surfaces and found strong spectral differences caused by the substrates. This holds not only for the π^* resonances below the C 1s ionization threshold but also for the σ-type resonances above threshold. In addition, the medium-resolution spectra presented by Weiss et al. [3] show also substrate-dependent changes in the energy region of the weak σ-type resonances below threshold. It is, therefore, important to have a clear understanding of the character of these resonances in order to interpret future high-resolution spectra performed at third-generation synchrotron radiation facilities correctly. This lack of clarity in the assignment is accompanied by the lack of state-of-the-art calculations of the NEXAFS spectrum of this molecule.

In this Letter, we present high-resolution NEXAFS gas-phase spectra of C_6H_6 and C_6D_6 in combination with ab initio density functional theory (DFT) calculations. Since the NEXAFS spectra were measured by detecting the total photoionization yield, we will refer to them as photoionization spectra in the following. The vibrational fine structure of C_6H_6 and C_6D_6 in combination with molecular orbital plots obtained from the DFT calculations allow to derive detailed information about the character of the corresponding peaks B and C.

2. Experimental setup

The photoionization spectrum of benzene was measured at the 10.0.1 undulator beamline at the advanced light source (ALS) in Berkeley, CA, which is equipped with a spherical-grating monochromator. Complimentary measurements on benzene-d_6 (C_6D_6) were made at beamline UE56/2-PMG1 at BESSY II in Berlin, Germany. The spectra were obtained by detecting the total photoionization yield with a gas cell that contains two parallel plates for the collection of the charged particles [13]. The photoionization cell was filled with approximately 35 μbar of benzene and it was separated from the ultra-high vacuum of the monochromator by a 1000-Å thick aluminum window. In order to avoid the accumulation of impurities in the gas in the form of fragmentation products formed by the deexcitation process, the measurements were performed with a constant gas flow through the gas cell. The spectra were measured with a spectral resolution better than 65 meV.

The spectrum of benzene measured at beamline 10.0.1 was calibrated by shifting the nominal energy positions of the prominent lines of the C $1s \rightarrow \pi^*$ transitions to the calibrated values obtained from medium-resolution spectra that had been measured before at the plane-grating monochromator SX700/II at BESSY. The latter spectra as well as the spectra of C_6D_6 measured at the plane-grating monochromator UE56/2-PGM1 were calibrated using the well-known energy position of the $v'' = 0 \rightarrow v' = 0$ transition of the N $1s \rightarrow \pi^*$ excitation in N_2 at 400.88 eV [14], together with the relation $\Delta E \propto E^{3/2}$ valid for plane-grating monochromators; here ΔE describes the difference between the measured and the actual energy positions. In this way an energy accuracy of better than 30 meV was obtained and the energy scale agrees well with that given by Rennie et al. [10].

3. Computational details

Quantum chemical calculations were performed to assign the observed peaks in the experimental NEXAFS spectra. The theoretical X-ray absorption spectra were generated using Slater's transition-state method (TS) [15,16] in combination with a double basis set technique [17]. These results were then improved by ΔKohn–Sham (ΔKS) DFT calculations.

In a first step, a geometry optimization was performed. The molecular basis sets consist of a triple-zeta

valence plus polarization (TZVP) basis [18] in a [4s, 3p] contraction with one added d function for carbon and a primitive (5s) basis set augmented with one p function and contracted to [3s, 1p] for hydrogen [19]. For the calculations of the spectrum, the orbitals of the ionized carbon center were described by an IGLO-III basis [20] in order to obtain an improved representation of relaxation effects in the inner orbitals, while the remaining carbon atoms were described by valence basis sets together with effective core potentials (ECPs) [21]. This simplifies the definition of the core hole state since the use of an ECP description eliminates the 1s level of the carbon atom to which it is applied. The use of ECPs leads only to negligible effects on the computed spectrum, see [22]. In addition, a large [19s, 19p, 19d] diffuse even-tempered basis set [17], centered at the ionization site, was added to account for unbound resonance states near this site. The spectrum was then calculated by a gaussian convolution of the discrete spectrum with an energy-dependent broadening. For the region below the ionization threshold, the broadening (full width at half maximum, FWHM) was set to 0.2 eV, while a linear increase up to a width of 4.5 eV was assumed for higher energies, as is common practice in the analysis of experimental NEXAFS spectra [8].

The DFT TS calculation reproduces most of the relaxation effects upon core ionization and provides a single set of orthogonal orbitals for the spectrum calculation. In order to determine the absolute energy position of the spectrum, ΔKS calculations were performed to obtain the fully relaxed ionization potential (IP). The difference of the resulting IP value and its TS approximation was used to correct the energy scale of the spectrum.

The DFT TS calculation of the spectrum assumes a frozen molecular ion density and thus neglects relaxation effects of the ionic molecular core upon adding the excited electron. This effect is largest for the valence-type π^* excitations. Therefore, these states were determined by fully relaxed final-state calculations. A sequence of the most prominent excitations into antibonding orbitals of σ-symmetry and Rydberg orbitals were calculated analogously. The corresponding peaks in the TS spectrum have been shifted to include relaxation effects obtained from the fully relaxed final-state calculations.

All excitation energies were calculated for the geometry of the ground state, i.e. no geometry optimization for the core-excited state was performed. A geometry optimization for the C $1s^{-1}\pi^*e_{2u}(b_1)$ state resulted in a reduction of the theoretical excitation energy by only 200 meV and provides an estimate of the uncertainty. The entire spectrum was shifted by 0.2 eV to higher energies [23] to take relativistic effects into account.

All DFT calculations were performed using the StoBe density functional theory code [24] with the gradient-corrected RPBE exchange/correlation functional [25,26].

4. Results and discussion

Fig. 1 shows the experimental and theoretical NEXAFS spectrum of benzene below the C 1s ionization threshold revealing very good agreement. The experimental spectrum consists of four main structures (labeled A–D) which all exhibit vibrational fine structure. This fine structure explains the differences in widths and peak heights between the experimental and theoretical spectra. The present experimental spectrum of benzene given in Fig. 1 matches well with a previous high-resolution spectrum reported by Rennie et al. [10]. The spectra of benzene and benzene-d_6 in the region of peaks B and C are shown in more detail in the inset of Fig. 1; they exhibit minor variations that are caused predominantly by the differences in the vibrational energies, $\hbar\omega_i$, of the individual vibrational modes. The excitation energies of the $v'' = 0 \rightarrow v' = 0$ transitions (bold arrows in Fig. 1) in benzene-d_6 are slightly lower than in benzene, by 10 meV (peak A) up to 60 meV (peak C). The differences can be understood by changes in the zero-point energies $\frac{1}{2}\hbar\omega = \sum_{i=1}^{30}\frac{1}{2}\hbar\omega_i$ upon excitation or by differences in the minima of the potential energy surfaces caused by terms beyond the Born–Oppenheimer approximation. This clearly shows that nuclear motion has to be taken into account for a proper description of the excitation energies. This influence of nuclear motion on the excitation energies will certainly also contribute to the observation that the experimental excitation energies are higher than the calculated values by ≅ 150–200 meV.

Peaks A and D have been assigned in the literature to the transitions C $1s^{-1}\pi^*e_{2u}$ and C $1s^{-1}\pi^*b_{2g}$, respectively. The assignments given in the literature for peaks B and C agree only in assigning σ-symmetry to the final-state orbitals, i.e., they exhibit no node in the molecular plane. The detailed character of these orbitals, however, has been described quite differently, as summarized in Table 1.

In the presence of a localized core hole, the symmetry of benzene is reduced from D_{6h} to C_{2v}. In this case, the degenerate orbital e_{2u} (peak A) splits into two orbitals with b_1 and a_2 symmetry. Furthermore, an excitation from the localized core hole into the a_2 orbital is forbidden by dipole-selection rules. Thus, the main peak A at 285.1 eV can be assigned to the C $1s^{-1}\pi^*e_{2u}(b_1)$ transition. This transition exhibits a rich fine structure caused by the excitation of different vibrational modes; it is discussed in [6,10]. In addition, a high-energy shoulder A′ at ≅ 286.2 eV is observed. This shoulder cannot be explained by vibrational excitations of the C $1s^{-1}\pi^*e_{2u}(b_1)$ transition [10]. Its energy position agrees well with the value calculated for the dipole-forbidden C $1s^{-1}\pi^*e_{2u}(a_2)$ transition. This excitation was originally suggested by Schwarz et al. [12] and tentatively assigned to the discussed spectral feature by Rennie et al. [10]. The present calculations strongly support the assign-

Table 1
The present assignment of peaks A–D together with selected assignments from the literature, where a question mark '?' indicates tentative assignments. For the well-resolved resonances, the $v'' = 0 \rightarrow v' = 0$ excitation energies, E_{ex}, are also given together with the theoretical values, E_{th}

Peak	$E_{ex}^{C_6H_6}$ (eV)	$E_{ex}^{C_6D_6}$ (eV)	E_{th} (eV)	Ref. [10]	Ref. [11]	Ref. [12]	Present work
A	285.11	285.10	284.97	$\pi^* e_{2u}(b_1)$	$\pi^* e_{2u}$	$\pi^* e_{2u}(b_1)$	$\pi^* e_{2u}(b_1)$
A′			285.91	$\pi^* e_{2u}(a_2)$?		$\pi^* e_{2u}(a_2)$?	$\pi^* e_{2u}(a_2)$
B	287.17	287.14	286.92	3s	Rydberg + σ^*(C–H)	Rydberg + σ^*(C–H)	σ-like valence + some Rydberg
C	287.92	287.86	287.78	3p/3d?	Rydberg	3p(s,d)	σ-like valence + some Rydberg
D				$\pi^* b_{2g}$, 4s, 4p	$\pi^* b_{2g}$	$\pi^* b_{2g}$, 3d, 4s, 4p	$\pi^* b_{2g}$+Rydberg

ment to this dipole-forbidden resonance, and the intensity can be explained by vibronic coupling. Similar results have been found for the N $1s^{-1}\pi^* a_2$ excitation of pyridine [8], which has the same molecular symmetry as benzene with a localized core hole.

In the literature, peaks B and C were partly assigned to excitations into pure Rydberg orbitals or to mixed valence/Rydberg excitations. However, the authors normally do not specify their definition of Rydberg orbitals which is probably part of the reason for the different assignments given for these peaks. Here we consider Rydberg orbitals as diffuse orbitals whose spatial extent is considerably larger than the diameter of the C_6H_6 molecule of $\cong 5$ Å . Electrons in these Rydberg orbitals overlap only little with the molecular core and, therefore, these orbitals are non-bonding. As a result, the geometry and vibrational fine structure of core-to-Rydberg excitations should be very similar to those of core-ionized states. Our definition of Rydberg orbitals agrees with that of Yagishita et al. [7], but differs from the definition by Bagus et al. [27]. The latter authors define a molecular Rydberg orbital only by its size in relation to that of a corresponding atomic Rydberg orbital. This definition ignores the fact that molecular orbitals of 'atomic Rydberg orbital extent' can still couple with other molecular orbitals and can therefore admix covalent character. For example, a 3s or 3p electron in a free carbon atom sees, in good approximation, the ionic C^+ core as a point charge, whereas an electron in benzene, located in an orbital comparable in size to an atomic 3s or 3p orbital, experiences an extended $C_6H_6^+$ core. The latter orbital will thus be modified as compared to an atomic 3s or 3p orbital and can assume some covalent character that may affect the molecular geometry. Such admixing of valence orbitals to low-*n* Rydberg orbitals has been found in a number of small core-excited molecules like O_2 [7]. In larger molecules like C_6H_6 this effect is expected to be more pronounced.

In the literature, peak B has been assigned to a C $1s^{-1}3s$ Rydberg state (e.g. [10]) or to a C $1s^{-1}3s\sigma^*$(C–H) mixed state (e.g. [11]). The vibrational structure of this state is shown in detail in the inset of Fig. 1. It is dominated by a spacing of $\cong 120$ meV which can be related to the C–C stretching modes. However, the intensity distribution for the vibrational substates differs considerably from that obtained for the core-ionized state shown in Fig. 4 of [10]; this photoelectron spectrum is also dominated by the C–C stretching modes, but with much less intense higher vibrational excitations. Based on these differences in the vibrational structure we can conclude that the equilibrium geometry of the core-excited and the core-ionized state is different. Thus the occupation of the final-state orbital influences the molecular bonds by assuming some valence character. This agrees well with plots of the final-state orbitals obtained from the present calculations. Fig. 2a

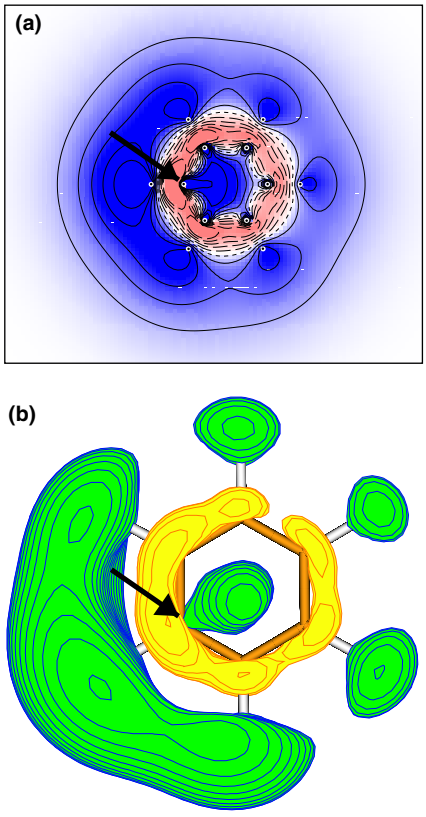

Fig. 2. Plots of the final-state orbitals corresponding to peak B: (a) contour-line plot along the molecular plane; (b) orbital-surface plot with atom bonds indicated by sticks. The arrows indicate the position of the localized core hole.

shows a contour-line plot along the molecular plane and Fig. 2b gives the corresponding orbital-surface plot. The final-state orbital has two radial nodes in the molecular plane. A Mulliken population analysis [28] shows strong *s* contributions at the core-excited carbon atom and *p* contributions for all other C atoms. In addition, *s* contributions at the H atoms can be found. The orbital exhibits an overall σ(C–C) bonding character and an antibonding character along the C–H bonds. In addition, significant electron density can be found outside the region defined by the H atoms; this defines the admixture of Rydberg character to the orbital.

In the literature peak C has been mainly assigned to an excitation into a Rydberg orbital. Rennie et al. [10] suggested tentatively two Rydberg excitations in this energy region, namely C $1s^{-1}3p$ and C $1s^{-1}3d$. However, the present DFT-calculations do not support the presence of an additional excitation with significant intensity in this energy region. A detailed comparison of the spectra of C_6H_6 and C_6D_6 shown in the inset of Fig. 1 exhibits a considerable shift of the spectral feature c′ to lower energies, i.e. it cannot be assigned to a pure electronic transition. Taking into account an energy splitting of ≅ 400 meV between the peaks C and c′, the latter can be assigned to a C–H stretching vibrational mode. This demonstrates that the vibrational fine structure of peak C differs from that of the C $1s^{-1}$ photoelectron spectrum [10], i.e. the excited orbital has sizeable valence character. Fig. 3 shows the molecular-orbital plot for the excited-state orbital corresponding to peak C. A population analysis of this orbital yields strong *p* contributions at all C atoms as well as *s* contributions at the H atoms. The nodal structure of this orbital reveals antibonding σ*(C–C) and σ*(C–H) character. The antibonding character is particularly strong along the bond between the excited C atom and the adjacent H atom and explains the presence of the C–H stretching vibrational mode in the spectrum. In addition, we also find some Rydberg character for this orbital.

The overall size of the two σ-type final-state orbitals is larger than those of the π-orbitals. However, there is still a large electron density close to the atoms which gives these orbitals valence character. In summary, these orbitals have to be described as σ-type orbitals with σ(C–C) (peak B) or σ*(C–C) (peak C), σ*(C–H), plus some admixed Rydberg character. The high electron density close to the C atoms explains the high excitation cross section [29]. The present characterization of the σ-type orbitals is also supported by calculations that are performed without a diffuse basis set which is necessary to obtain a correct description of Rydberg contributions (see above). The absence of Rydberg contributions in the basis set of the calculations does not lead to changes in the theoretical intensities or energy positions for these resonances.

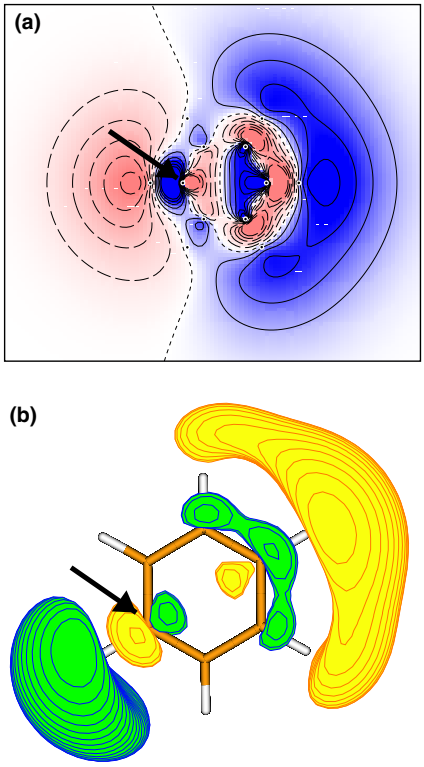

Fig. 3. Orbital plots of the final-state orbitals corresponding to peak C. For details, see Fig. 2.

The results are also fully in line with the condensed-phase spectra by Menzel et al. [11]. It is well known that extended Rydberg orbitals are very sensitive to external perturbers like neighboring atoms or molecules; the excitations into these orbitals are normally suppressed. However, in the present case of benzene the gas-phase and condensed-phase spectra differ only very little. This can readily be explained by the fact that the electron density distribution of these orbitals is determined by predominant valence character and is, thus, only weakly influenced by the neighboring molecules in solid benzene.

According to the calculations and in full agreement with previous studies peak region D consists of one main peak as well as a number of very weak resonances. The main peak is due to a C $1s^{-1}\pi^*b_{2g}$ excitation, while the weak resonances can be assigned to core-to-Rydberg excitations.

5. Summary and conclusions

High-resolution photoionization spectra of C_6H_6 and C_6D_6 are presented together with DFT NEXAFS-calculations. The agreement between the experimental and theoretical results is excellent. This shows the suitability of DFT to describe well the NEXAFS spectra of small aromatic molecules and allows elucidation of the orbital character of the excited states of peaks B and C in more

detail. In both cases the orbitals are clearly assigned to σ-like mixed valence/Rydberg orbitals with bonding (peak B) and antibonding (peak C) character along the C–C bonds, antibonding character along the C–H bonds, and some Rydberg character. These findings agree well with the observed vibrational fine structure. Excitations into pure Rydberg orbitals give only minor contributions to the spectrum.

Acknowledgements

R.P. and C.K. gratefully acknowledge the group of Prof. U. Becker for providing some hours of their beamtime at beamline UE56/2-PGM1. This allowed us to promptly perform the complimentary measurements of C_6D_6 in the advanced stage of the work. The work at the Freie Universität Berlin was supported by the Deutsche Forschungsgemeinschaft, Project No. PU 180/1-1.

References

[1] A.P. Hitchcock, D.C. Newbury, I. Ishii, J. Stöhr, J.A. Horsley, R.D. Redwing, A.L. Johnson, F. Sette, J. Chem. Phys. 85 (1986) 4849.
[2] P. Väterlein, M. Schmelzer, J. Taborski, T. Krause, F. Viczian, M. Bässler, R. Fink, E. Umbach, W. Wurth, Surf. Sci. 452 (2000) 20.
[3] K. Weiss, S. Gebert, M. Wühn, H. Wadepohl, Ch. Wöll, J. Vac. Sci. Technol. A 16 (1998) 1017.
[4] L.G.M. Pettersson, H. Ågren, Y. Luo, L. Triguero, Surf. Sci. 408 (1998) 1.
[5] R. Radhakrishnan, C. Reed, S.T. Oyama, M. Seman, J.N. Kondo, K. Domen, Y. Ohminami, K. Asakura, J. Phys. Chem. B 105 (2001) 8519.
[6] Y. Ma, F. Sette, G. Meigs, S. Modesti, C.T. Chen, Phys. Rev. Lett. 89 (1989) 2044.
[7] A. Yagishita, E. Shigemasa, N. Kosugi, Phys. Rev. Lett. 72 (1994) 3961.
[8] C. Kolczewski, R. Püttner, O. Plashkevych, H. Ågren, V. Staemmler, M. Martins, G. Snell, A.S. Schlachter, M. Sant'Anna, G. Kaindl, L.G.M. Pettersson, J. Chem. Phys. 115 (2001) 6426.
[9] A.P. Hitchcock, M. Pocock, C.E. Brion, M.S. Banna, D.C. Frost, C.A. McDowell, B. Wallbank, J. Electron Spectrosc. Relat. Phenom. 13 (1978) 345.
[10] E.E. Rennie, B. Kempgens, H.M. Köppe, U. Hergenhahn, J. Feldhaus, B.S. Itchkawitz, A.L.D. Kilcoyne, A. Kivimäki, K. Maier, M.N. Piancastelli, M. Polcik, A. Rüdel, A.M. Bradshaw, J. Chem. Phys. 113 (2000) 7362.
[11] D. Menzel, G. Rocker, H.-P. Steinrück, D. Coulman, P.A. Heimann, W. Huber, P. Zebisch, D.R. Lloyd, J. Chem. Phys. 96 (1992) 1724.
[12] W.H.E. Schwarz, T.C. Chang, U. Seeger, K.H. Hwang, Chem. Phys. 117 (1987) 73.
[13] M. Domke, T. Mandel, A. Puschmann, C. Xue, D.A. Shirley, G. Kaindl, H. Petersen, P. Kuske, Rev. Sci. Instrum. 63 (1992) 80.
[14] R.N.S. Sodhi, C.E. Brion, J. Electron Spectrosc. Relat. Phenom. 34 (1984) 363.
[15] J.C. Slater, in: P.O. Loewdin (Ed.), Advances in Quantum Chemistry, Academic Press, New York, 1972, p. 1.
[16] J.C. Slater, K.H. Johnson, Phys. Rev. B 5 (1972) 844.
[17] H. Ågren, V. Carravetta, O. Vahtras, L.G.M. Pettersson, Theor. Chem. Acc. 97 (1997) 14.
[18] T.H. Dunning, J. Chem. Phys. 55 (1971) 716.
[19] S. Huzinaga, J. Chem. Phys. 42 (1965) 1293.
[20] W. Kutzelnigg, U. Fleischer, M. Schindler, NMR – Basic Prinicples and Progress, vol. 23, Springer, Heidelberg, 1990, p. 165.
[21] L.G.M. Pettersson, StoBe basis set library, see Ref. [24].
[22] L.G.M. Pettersson, U. Wahlgren, O. Gropen, Chem. Phys. 80 (1983) 7.
[23] L. Triguero, O. Plashkevych, L.G.M. Pettersson, H. Ågren, J. Electron Spectrosc. Relat. Phenom. 104 (1999) 195.
[24] The program package StoBe is a modified version of the DFT-LCGTO program package DeMon, originally developed by A. St.-Amant and D. Salahub (University of Montreal), with extensions by K. Hermann and L.G.M. Pettersson.
[25] B. Hammer, L.B. Hansen, J.K. Nørskov, Phys. Rev. B 5 (1999) 7413.
[26] J.P. Perdew, K. Burke, M. Ernzerhof, Phys. Rev. Lett. 77 (1996) 3865.
[27] P.S. Bagus, K. Weiss, A. Schertel, Ch. Wöll, W. Braun, C. Hellwig, C. Jung, Chem. Phys. Lett. 248 (1996) 129.
[28] R.S. Mulliken, J. Chem. Phys. 23 (1955) 1833.
[29] J. Stöhr, NEXAFS Spectroscopy, Springer, Berlin, 1992, p. 92.